UCRL-52690

OPTIMUM FREQUENCIES FOR REGIONAL DETECTION OF CAVITY-DECOUPLED EXPLOSIONS

Howard C. Rodean

March 21, 1979

Work performed under the auspices of the U.S. Department of Energy by the UCLLL under contract number W-7405-ENG-48.

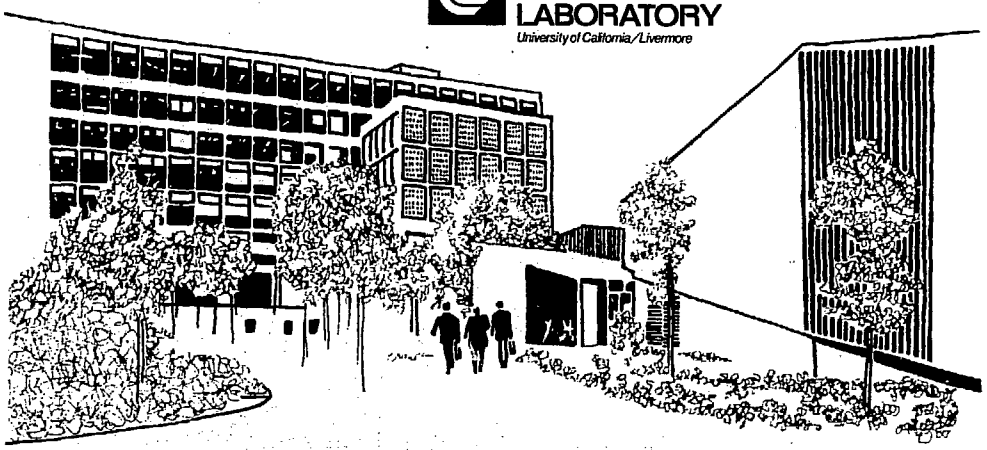

Distribution Category
UC-11

LAWRENCE LIVERMORE LABORATORY
University of California Livermore, California 94550

UCRL-52690

OPTIMUM FREQUENCIES FOR REGIONAL DETECTION OF CAVITY-DECOUPLED EXPLOSIONS

Howard C. Rodean

MS. date: March 21, 1979

OPTIMUM FREQUENCIES FOR REGIONAL DETECTION OF CAVITY-DECOUPLED EXPLOSIONS

ABSTRACT

This report examines the natures of compressional (P) waves that originate in the crust, propagate in the crust and upper mantle, and are observed as Pg, Pn, and $\bar{P}$ waves at regional distances. The discussion includes the observed variations of amplitude with epicentral distance for these waves as well as an estimate of values for the specific dissipation function Q_α in different regions. We studied theoretical source and propagation functions for direct, reflected, and head waves as approximations for the observed Pg, $\bar{P}$, and Pn, respectively. We conclude that the classical (critically refracted) head wave is not very significant in regional observations, and that the related interference head wave and diving wave are more likely observed as Pn. Using an assumed seismic noise spectrum and the constant Q_α model for seismic attenuation, we derive relations for the frequencies corresponding to maximum signal-to-noise ratio for the classical and interference head waves and for the direct, reflected, and diving waves. The relations among seismic frequency, epicentral distance, anelastic attenuation, and explosion yield are illustrated for a simple source and propagation model.

INTRODUCTION

The 0.5-to-5-Hz frequency band is optimum for detecting body waves from events at teleseismic distances. However, the potential use of regional seismic monitoring under a Comprehensive Test Ban Treaty has made it necessary to consider the use of higher frequencies. In addition, the possible use of cavity decoupling as an evasion technique has further increased the interest in higher frequencies because of some indications that cavity decoupling may be less effective at higher frequencies *(Springer et al., 1968)*.

In this study, we use some simple mathematical models for seismic wave propagation and seismic source and noise spectra to evaluate the effects of range, frequency, and explosion yield on seismic detection at regional distances. We emphasize two categories of compressional (P) waves: Pg and $\bar{P}$, which propagate in the crust at approximately 6 km/s, and Pn, which is critically or near-critically refracted at the Mohorovicic (M) discontinuity and propagates along the top of the mantle at velocities ranging from approximately 7.8 to 8.2 km/s. We consider seismic frequencies from 1 to 20 Hz and epicentral distances from 10 to 1,000 km.

THE NATURES OF SEVERAL CRUSTAL P WAVES

We are concerned with waves that originate in the crust, propagate in the crust and upper mantle, and are detected at epicentral distances of between 10 and 1,000 km. The P waves observed at these distances are determined by the earth's structure along their propagation paths which may penetrate to depths of approximately 200 km.

We assume the following continental model: a 1-km surface layer with an average P-wave velocity of 3 km/s, a granitic layer with an average P-wave velocity of 6 km/s, and the M discontinuity at a depth of 31 km, below which the P-wave velocity is approximately 8 km/s. In some areas, a basaltic layer with an average P-wave velocity of 7 km/s lies

between the granitic layer and the M discontinuity. The interface between the granitic and basaltic layers is the Conrad (C) discontinuity. For this part of our study, we assume the C discontinuity is at a depth of 16 km. Except for the surface layer, this model (Fig. 1) is identical with that in Fig. 81 in *Bath* (1973).

For our earth model, Pg with a velocity of 6 km/s is the first arrival at epicentral distances from 10 to approximately 100 km, P* with a velocity of 7 km/s is the first arrival between approximately 100 and 150 km, and Pn with a velocity of 8 km/s is the first arrival at greater regional distances (Fig. 1). If the C discontinuity is absent, Pg is the first arrival at distances less than approximately 150 km.

There is no question about the nature of Pn: it is a head wave that is critically or near-critically refracted at the M discontinuity. The literature gives two significantly different definitions for Pg. *Berry and West* (1966) and *Hill* (1971) defined Pg as a head wave that is critically or near-critically refracted at the top of the granitic layer, just as Pn is refracted at the top of the mantle. On the other hand, *Bath* (1973) implied in Fig. 81 that Pg is a direct wave by showing Pg radiated from a source at a depth of 8 km in the granitic layer. *Nersesov and Rautian* (1964) defined the first arrival at distances to 100 or 150 km as a direct P wave. We conclude that the definition of Pg as a direct or head wave depends on source depth and earth structure. Berry and West and Hill were considering seismic refraction data from surface and near-surface explosions; in such cases the source is in the low-velocity surface layer and Pg is formed by critical or near-critical refraction at the top of the granitic layer. As previously noted, Bath assumed a source at a depth of 8 km in the granitic layer. Nersesov and Rautian used data from earthquakes at depths of 5 to 20 km. For sources in the granitic layer, Pg is generated directly by the source. Therefore, the nature of Pg (direct or head wave) is a function of the source location with respect to the interface between the low-velocity surface layer and the granitic layer. All the above-cited authors are consistent in defining P* as a wave that is critically or near-critically refracted at the C discontinuity. In the remainder of this paper, we do not consider P* and our earth model does not include the C discontinuity.

The P waves following the first arrivals may be greater or smaller in amplitude than Pg and Pn. One secondary arrival, $\overline{P}$, is of particular interest because it follows Pn and is significantly stronger than Pn in some regions. It appears to be a kinematic extension of Pg because it propagates at approximately the same velocity, 6 km/s. It is called Pg instead of $\overline{P}$ in

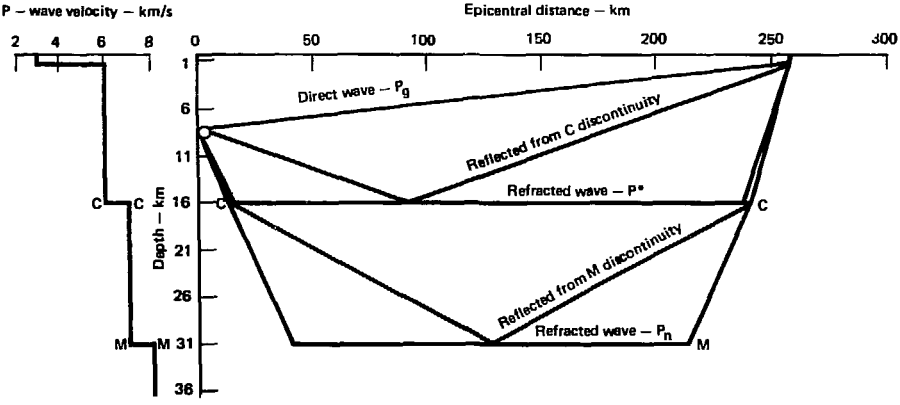

FIG. 1. Representative crustal model and some of the regional P waves from a source at a depth of 8 km.

some references (e.g. Nersesov and Rautian, *Evernden*, 1967). Nersesov and Rautian described Pg($\bar{P}$) as a wave that is generated by multiple reflections from the earth's surface and the base of the crust; they noted that the frequency content of these waves appears to be related to the local nature of the M discontinuity (sharp or blurred). *Haskell* (1966) concluded that $\bar{P}$ at long ranges should not be regarded as a direct wave but as an interference pattern produced by the superposition of a large number of higher-order modes (or a superposition of many multiply reflected and refracted waves). He also concluded that a low surface velocity and a steep velocity gradient at shallow depths are apparently sufficient for adequate entrapment of short-period P-wave energy.

THE PROPAGATION OF PG, PN, AND $\bar{P}$

OBSERVATIONS

Pg Waves

Nuttli (1978) determined the decay of amplitude with epicentral distance of 10-Hz, 6-km/s P waves at ranges of 10 to 200 km in the New Madrid seismic zone in the eastern United States (EUS) to be

$$A = A_0\Delta^{-1.4},$$

where

A_0 reference amplitude,
Δ epicentral distance.

For direct P in crystalline rocks at ranges to 150 km, Nersesov and Rautian found that

$$A = A_0\Delta^{-1.1} \text{ to } A = A_0\Delta^{-1.7}$$

for crystalline rocks, and for sedimentary rocks,

$$A = A_0\Delta^{-1.7} \text{ to } A = A_0\Delta^{-2.1}.$$

These data were obtained along segments of a 3,500-km profile in the southeastern USSR from the Pamirs to the Lena River.

Pn Waves

Nersesov and Rautian presented amplitude-vs-distance data for Pn, but they did not establish any average distance-amplitude relations because of wide variations in Pn behavior from region to region (seismically active regions of Central Asia, Kazakhstan, Altai, Sayan, and Pribaikal). Evernden found distinctly different Pn propagation in the EUS and the western United States (WUS). For 7.9-km/s Pn waves at epicentral distances of 200 to 1,000 km in the WUS,

$$A = A_0\Delta^{-3.6};$$

and for 8.5-km/s Pn waves at ranges of 200 to 2,000 km in the EUS,

$$A = A_0\Delta^{-2}.$$

$\bar{P}$ Waves

Nersesov and Rautian found that 6-km/s Pg($\bar{P}$) waves propagate as follows at epicentral distances of 200 to 500 km:

$$A = A_0\Delta^{-2}.$$

Evernden found the following relation for 6-km/s Pg($\bar{P}$) waves at epicentral distances of 200 to 1,000 km in the WUS, with amplitudes about 10 times those of Pn:

$$A = A_0\Delta^{-3}.$$

$\bar{P}$ is not a well-defined phase in the EUS (Evernden).

SPECIFIC DISSIPATION FUNCTION Q_α

In principle, the above empirical amplitude-distance relations could be replaced by the following equation to separate geometric and anelastic attenuation effects:

$$A = A_0\Delta^{-m-n} \qquad (1)$$

where

m = geometric attenuation coefficient,
n = anelastic attenuation coefficient.

A more appropriate relation with respect to the physics of attenuation is

$$A = A_0 \Delta^{-m} \exp - \pi \Delta f / \alpha Q_\alpha \qquad (2)^*$$

where

f = frequency (Hz),

Q_α = specific dissipation function for compressional waves,

α = compressional wave velocity.

If the attenuation functions Δ^{-n} [Eq. (1)] and $\exp - \pi \Delta f / \alpha Q_\alpha$ [Eq. (2)] are tangent at epicentral distance Δ (i.e., the slopes $d(\ln A)/d(\ln \Delta)$ of the two functions are equal), we can derive the following relation between Q_α and n:

$$Q_\alpha = \pi \Delta f / \alpha n. \qquad (3)$$

The value of $\bar{Q}_\alpha$ corresponding to the mean value of Q_α^{-1} in the epicentral range between Δ_1 and Δ_2 is

$$\bar{Q}_\alpha = \pi (\Delta_2 - \Delta_1) f / \alpha n \ln(\Delta_2 / \Delta_1) . \qquad (4)$$

Solutions of Eq. (4) for $\bar{Q}_\alpha$, based on the following assumptions for m, are summarized in Table 1 for the empirical relations given by *Nuttli* (1978), *Nersesov and Rautian* (1964) and *Evernden* (1967):

Pg–m = 1, assuming spherical far-field radiation;

Pn–m = 2, assuming epicentral distances much greater than the critical distance for head waves ($m \geq 2$, see p. 147 and Fig. 3.23, *Cerveny and Ravindra*, (1971);

$\bar{P}$–m = 5/6, assuming $\bar{P}$ is an Airy phase; m = 1 otherwise (*Ewing et al.*, 1957, p. 145).

DISCUSSION

We must note that the solutions of Eq. (4) for $\bar{Q}_\alpha$ corresponding to the mean values of Q_α^{-1} that are presented in Table 1 are not unique, but are functions of the assumed seismic frequencies. We must also recognize that the effects of geometric and anelastic attenuation are not necessarily as separable and as simple as implied by Eqs. (1 through 4). It is more appropriate to regard the solutions of Eq. (4) as apparent values of Q_α. We consider this problem on a case-by-case basis.

Pg Waves

Nuttli (1978) applied an analog of Eq. (2) to his data for Lg, but he did not attempt to estimate $\bar{Q}_\alpha$ for Pg: "It is customary to fit close-in P-wave data by an empirical equation such as ($A = A_0 \Delta^{-N}$), even though that equation does not take account of the source radiation pattern, anelasticity, and constructive interference of reflected and refracted waves.

*Note that Δ in Δ^{-m} is a dimensionless distance but Δ in $\exp - \pi \Delta f / \alpha Q \alpha$ has the dimension of length (e.g., km).

TABLE 1. Estimated values of $\bar{Q}_\alpha$ for Pg, Pn, and $\bar{P}$.

Wave	Reference	Location	Δ_1 (km)	Δ_2 (km)	m+n	m	n	f (Hz)	α (km/s)	$\bar{Q}_\alpha$
Pg	*Nuttli* (1978)	EUS	10	200	1.4	1.0	0.4	10	6	830
	Nersesov and Rautian (1964)	SE-USSR	10	150	1.4[a]	1.0	0.4	2.5[c]	6	170
					1.9[b]	1.0	0.9	2.5[c]	6	75
Pn	*Evernden* (1967)	WUS	200	1,000	3.6	2.0	1.6	1[d]	7.9	123
		EUS	200	2,000	2.0	2.0	0	1[d]	8.5	∞
$\bar{P}$	*Nersesov and Rautian* (1964)	SE-USSR	200	500	2.0	0.8	1.2	25[c]	6	357
	Evernden (1967)	WUS	200	1,000	3.0	0.8	2.2	1[d]	6	118

[a]Crystalline rocks.

[b]Sedimentary rocks.

[c]Geometric mean of instrument band width of 0.1- to 1.5-s period.

[d]Assumed for narrow-band short-period instruments used.

The scatter in the P-wave amplitude data, which can be as large as an order of magnitude, can be attributed to these and other phenomena such as scattering and soil amplification." The value of $\bar{Q}_\alpha = 830$ is comparable to the results of *Herrmann and Mitchell* (1975), who used surface-wave data to determine values for Q_β for shear waves in the crust in the EUS. They found that $\bar{Q}_\beta \simeq 350$ in the upper 17 km and $\bar{Q}_\beta \simeq 1000$ in the lower 20 km of the crust. These values for $\bar{Q}_\beta$ imply approximate values for $\bar{Q}_\alpha$ of 700 and 2,000, respectively. The values of $\bar{Q}_\alpha = 170$ and $\bar{Q}_\alpha = 75$ from Nersesov and Rautian's data are much lower, but would be 680 and 300, respectively, if a frequency of 10 Hz were assumed. Nersesov and Rautian stated that the instrument response was flat in the period range from 0.1 to 1.5 s, but they did not give any frequency data for the observed signals. The assumed 2.5-Hz frequency corresponds to the geometric mean of the bandwidth. It is quite possible that a frequency closer to 10 Hz than 2.5 Hz is appropriate for the Pg data of Nersesov and Rautian.

Pn Waves

The values for the apparent $\bar{Q}_\alpha$ for Pn based on Evernden's relations range from 123 in the WUS to infinity in the EUS. If we take infinity to mean a high, positive value, these results are in general agreement with the conclusions of *Der and McElfresh* (1977), who found that Q_α at the top of the mantle is low (approximately 100 to 200) in the WUS and high (approximately 1500 or more) in the EUS. However, we should note the admonition of *Cerveny* (1966) that "there is practically no sense in determining the absorption coefficients from the amplitude curves of head waves." Subsequently, *Hill* (1973) obtained additional theoretical results that "emphasize Cerveny's observation that the pure head wave is a fragile entity. Its character is destroyed by small velocity gradients in the refracting medium as well as by slight curvature of the refracting boundary." Hill considered a spherically symmetrical earth model with velocity and density discontinuities at a spherical boundary (corresponding to the M discontinuity). He studied the effects of velocity gradients below this boundary on P-wave propagation and obtained the following results:

(1) A critical negative (with increasing depth) velocity gradient exists for which critically refracted waves in a spherical earth have the same form as the classical head wave for flat, homogeneous layers.

(2) The amplitudes of critically refracted waves decay more rapidly with distance than the classical head wave if the velocity gradient is more negative than the critical value.

(3) For velocity gradients that are positive, null, or less negative than critical, the amplitudes of critically refracted waves decay less rapidly with distance than the classical head wave. Hill used the above properties together with published Pg (as a head wave, not as a direct wave), P*, and Pn amplitude data to infer some bounds on anelasticity and velocity gradients in the crust and mantle lid. The Pg and P* data were for the continental US; the Pn data were for a site near Hawaii. He found, consistent with published heat flow data, that velocity gradients are negative in the Basin and Range Province of the WUS and are positive in the EUS. He also obtained apparent values for Q_α in the crust of less than 1,000 in the Basin and Range Province and greater than 1,000 or even negative in the EUS. Our values of 123 in the WUS and infinity in the EUS are consistent with Hill's results.

$\bar{P}$ Waves

Press (1964) analyzed Pg($\bar{P}$) data from NTS explosions and obtained an average value of $\bar{Q}_\alpha = 260 \pm 40$, a value somewhat higher than our value of $\bar{Q}_\alpha = 118$ for $\bar{P}$ in the WUS. Press used the Lg-wave velocity of 3.5 km/s in determining $\bar{Q}_\alpha$; using 6 km/s changes his value from 260 to 150, a value closer to ours. Press considered his value of $\bar{Q}_\alpha$ for $\bar{P}$ to be a minimal value because the effects of scattering and leaking modes were neglected. *Haskell* (1966) analyzed the leakage attenuation of $\bar{P}$ and concluded that $\bar{Q}_\alpha$ for anelastic attenuation in crustal rocks could be in the range of 500 to 1,000, and that leakage attenuation appears to be dominant in the observed rates of decay of $\bar{P}$.

CONCLUSIONS

The propagation of the crustal P waves (Pg, Pn, $\bar{P}$) is complicated by a variety of reflection and refraction phenomena that make it difficult to determine the $\bar{Q}_\alpha$ corresponding to anelastic attenuation. A range of 200 to 800 appears appropriate for determining the effect of anelastic attenuation on the detection of crustal P waves in the 1-to-20-Hz band.

SOURCE AND PROPAGATION FUNCTIONS FOR PG, PN, AND $\bar{P}$

We assume the flat earth model shown in Fig. 2: a 30-km homogeneous, isotropic crust with a compressional wave velocity of 6.4 km/s above an isotropic, laterally homogeneous mantle with a compressional wave velocity of 8 km/s at the M discontinuity. We will consider zero and finite velocity gradients with increasing depth in the mantle. This is identical with the models analyzed by *Cerveny and Ravindra* (1971) and by *Hill* (1973), except that Hill's model was that of a spherical earth. In addition, Hill analyzed acoustic waves in a fluid while Cerveny and Ravindra considered compressional and shear waves in a solid. In the following, we make extensive use of the work by Cerveny and Ravindra and some of Hill's results.

We will assume a time-harmonic point source of compressional waves in the crust of the form (*Cerveny and Ravindra*, 1971, Sec. 2.4) such that

$$\exp[i\omega(t - \tau)]\bar{n}_p$$

where

$\bar{n}_p$ = unit compressional wave vector,
t = time,
τ = travel time from source to receiver,
ω = angular frequency.

Cerveny and Ravindra [Eq. (3.1)] give the following relation for the far-field radiation in the source region (a model for the direct wave Pg):

$$\bar{W}^1 = (1/r) \exp[i\omega(t - \tau_1)]\bar{n}_p \qquad (5)$$

where

$$\tau_1 = r/\alpha_1 \qquad (6)$$

and

r = radial distance between source and receiver,
$\bar{W}^1$ = displacement vector,
α_1 = compressional wave velocity in the crust.

Cerveny and Ravindra [Eqs. (2.147 through 2.149, 3.2 through 3.5)] give the following equation

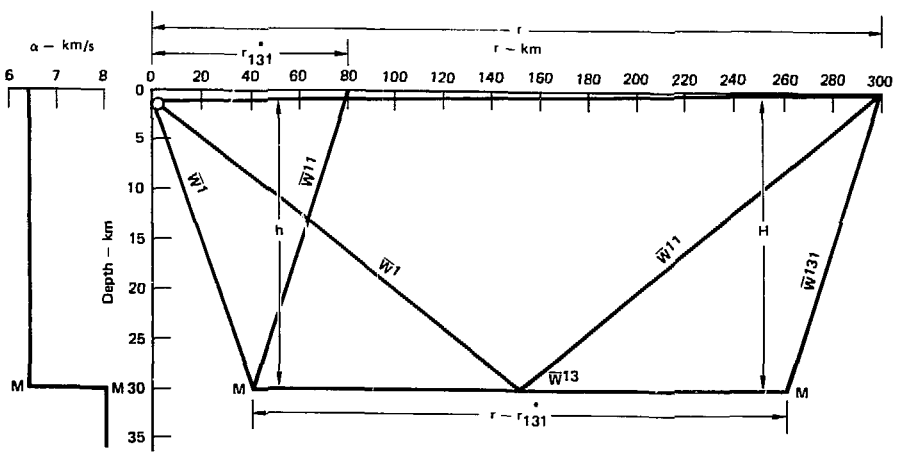

FIG. 2. Earth model used for direct, reflected, head (classical and interference), and diving wave solutions by Cerveny and Ravindra (1971). They also assumed $\beta_1/\alpha_1 = \beta_2/\alpha_2 = 0.577$, $\rho_1/\rho_2 = 1$ and b (mantle temperature gradient parameter) = 0.00283/km for the numerical examples mentioned in this report. Unlike this sketch, they assumed h = H = 30 km. The effect of h = 29 km vs h = 30 km is negligible for the problems considered in this report.

for a compressional wave that is reflected once from the M discontinuity (a rough approximation to a $\bar{P}$ model):

$$\bar{W}^{11} = (R_{11}/L)\,[\exp i\omega(t - \tau_{11})]\bar{n}_p \qquad (7)$$

where

$$L = [r^2 + (h+H)^2]^{1/2} \qquad (8)$$

$$\tau_{11} = L/\alpha_1 \qquad (9)$$

and

h = height of source above the M discontinuity,

H = height of receiver above the M discontinuity,

L = reflected ray-path length,

r = epicentral distance,

R_{11} = reflection coefficient [$-1 < R_{11} < 0$, Cerveny and Ravindra, Eq. (2.74)].

For the classical head wave (Pn), Cerveny and Ravindra [Eqs. (3.88, 3.90-3.92) give the solution which exists only for $r > r^*_{131}$] so that

$$\bar{W}^{131} = \frac{\alpha_1 \Gamma_{131} \exp[i\omega(t - \tau_{131})]\bar{n}_p}{i\omega r^{1/2}(r - r^*_{131})^{3/2}} \qquad (10)$$

where

$$r^*_{131} = \frac{\alpha_1(h+H)}{(\alpha_2^2 - \alpha_1^2)^{1/2}} \qquad (11)$$

$$\tau_{131} = \frac{r}{\alpha_2} + \frac{h+H}{\alpha_1}\left[1 - \left(\frac{\alpha_1}{\alpha_2}\right)^2\right]^{1/2} \qquad (12)$$

and

r = epicentral distance,

r^*_{131} = critical distance beyond which the headwave exists,

$r - r^*_{131}$ = distance the headwave propagates in the upper mantle,

α_2 = compressional wave velocity beneath the M discontinuity,

Γ_{131} = headwave coefficient (≈4.4 for our earth model, Cerveny and Ravindra, Fig. 3.8).

Ray theory was used to derive Eq. (10), which is not accurate in the vicinity of $r = r^*_{131}$ or in the adjacent interference zone ($r > r^*_{131}$) where the reflected wave and the head wave interfere with each other. Note that $\bar{W}^{131} \to \infty$ as $r \to r^*_{131}$. Wave theory gives more accurate results in this region (Cerveny and Ravindra, Secs. 7.23 through 7.25). Also note the term $(i\omega)^{-1}$ in Eq. (10) which is not present in Eqs. (5) and (7). The amplitude of the head wave is an inverse function of the incident wave, and if the amplitude spectrum of the incident wave is $|A(i\omega)|$, the amplitude spectrum of the head wave is $|A(i\omega)/i\omega|$. This is because the above direct and reflected P waves [Eqs. (5) and (7), respectively] are zero-order solutions of the form

$$\bar{W} = \exp[i\omega(t - \tau)]\bar{W}_0,$$

and the head wave is a first-order solution of the form

$$\bar{W} = \exp[i\omega(t - \tau)][\bar{W}_0 + (i\omega)^{-1}\bar{W}_1]$$ [Cerveny and Ravindra, Eqs. (2.3) and (2.4), respectively],

in which $\bar{W}_0 = 0$ [Cerveny and Ravindra (Eqs. 3.16, 3.18, and 3.22)]. This would suggest that we should use two different source functions in our study: one for Pg and $\bar{P}$, the other for Pn. However, we will see below that, for practical reasons, we need not be concerned about the $(i\omega)^{-1}$ term in Eq. (10).

First, we consider the head wave [Eq. (10)] with respect to the reflected wave [Eq. (7)]. By definition, the arrival times of the reflected and head waves coincide when $\tau_{11} = \tau_{131}$ and where [from Eqs. (8), (9) and (12)]

$$r(\tau_{11} = \tau_{131}) = r^*_{131} \; (= 80 \text{ km in our model}). \qquad (13)$$

For $r > r^*_{131}$, $\tau_{11} > \tau_{131}$, and there is interference between the reflected and head waves for some distance Δr_{131} beyond r^*_{131}. For wave durations δt such that the pulse length $\alpha_1 \delta t$ ranges from 1 to 3 km, Δr_{131} ranges from 26 to 47 km for our earth model (Cerveny and Ravindra, Table 3.3). Therefore, the head wave will not appear as a distinct first arrival (relative to the reflected wave) at distances less than $r^*_{131} + \Delta r_{131}$ (in our model, epicentral distances of approximately 105 to 130 km). Furthermore, the amplitude of the head wave is about one order of magnitude smaller than that of the head wave at the end of the interference zone

(Cerveny and Ravindra, p. 178). The amplitude ratio $|\bar{W}^{131}|/|\bar{W}^{11}|$ decreases rapidly with distance because of the differences of behavior of R_{11}/L in Eq. (7) and $\Gamma_{131} r^{-1/2} (r-r^*_{131})^{3/2}$ in Eq. (10). As $r_2 \to \infty$, $R_{11} \to -1$, $L \to r$, Γ_{131} remains constant, and $r^{1/2}(r - r^*_{131})^{3/2} \to r^2$.

Next, we consider the head wave with respect to the direct wave [Eq. (5)]. By definition, the arrival times of the direct and head waves coincide when $\tau_1 = \tau_{131}$. From Eqs. (6) and (12),

$$r(\tau_1 = \tau_{131}) = (h + H)\left(\frac{\alpha_2 + \alpha_1}{\alpha_2 - \alpha_1}\right)^{1/2}$$

(=180 km in our model). (14)

There is interference between the direct and head waves in the vicinity of $r = r(\tau_1 = \tau_{131})$, and the amplitude of the head wave is a small fraction of that of the direct wave at $r > r(\tau_1 = \tau_{131})$ (~6% at 180 km, ~2% at 360 km and ~1% at 540 km in our model).

In our ideal model, the amplitude of the classical head wave is much smaller, relative to the amplitudes of the direct and reflected waves, than is observed in practice. As we noted above, the Pg($\bar{P}$) wave amplitude is about ten times that of the Pn wave at an epicentral distance of 500 km in the WUS *(Evernden, 1967)*. Evernden also notes that Pg($\bar{P}$) is not well observed in the EUS. Let us speculate that this may be because Pn is as large or larger than Pg($\bar{P}$) in the EUS. Pn can be as large or larger than Pg and $\bar{P}$ if it is not a critically refracted classical head wave, but rather is a *near critically* refracted head wave. The conclusions of *Hill* (1971) are compatible with this hypothesis. He found evidence that the velocity gradients in the crust that affect Pg (as a head wave) and P* tend to be negative in the WUS and the positive in the EUS. *Cerveny* (1966) found that, for a flat-earth model, a positive (with increasing depth) velocity gradient of only 10 m/s/km is sufficient to form near critically refracted head waves that are one or two orders stronger than the classical head waves at distances of 150 km or more from the source. He also noted that the curvature of the M discontinuity has an effect similar to that of a positive velocity gradient, which is noticeable at distances of about 400 km. *Hill* (1973) concluded that, with a zero velocity gradient in the mantle, the earth's curvature has a significant effect on Pn amplitudes at distances as small as 200 to 300 km. The critical (negative) velocity gradient in a spherical earth that is required for the existence of a classical head wave is defined by the relation

$$\alpha(a) = (a/a_0)\alpha_2 \qquad (15)$$

where

$$a \leq a_0$$

and

a = radius from the center of the earth,
a_0 = radius of the M discontinuity,
α_2 = compressional wave velocity just below the M discontinuity.

In the remainder of this section, we follow the development in Ch. 6 of *Cerveny and Ravindra* (1971). We assume the flat-earth model of Fig. 2 with a positive velocity gradient below the M discontinuity which is defined by the relation [Cerveny and Ravindra, Eq. (6.1)]

$$\alpha(d) = \alpha_2(1 + bd) \qquad (16)$$

where

b = velocity gradient parameter ($b \geq 0$),
d = depth below the M discontinuity.

We are not interested in the case $b < 0$ except to note that the head wave decays more rapidly than the classical head wave if $b < 0$. The relation for a spherical earth [Eq. (15)] is equivalent to that for a flat earth [Eq. (16)] if $b = 0$.

The effect of a positive velocity gradient beneath the M discontinuity is illustrated in Fig. 3 (Cerveny and Ravindra, Figs. 6.1 and 6.2). A classical head wave that exists only if $b = 0$ is shown in Fig. 3(a); an interference head wave C+ that is formed by the near-critical refraction of a family of "diving" waves below the M discontinuity is shown in Fig. 3(b) for the case $b > 0$. The diving waves are named C_s waves where $s = 0, 1, 2, \ldots$, corresponding to the number of reflections from the underside of the M discontinuity. The angle of incidence of C_0 is slightly less than that of the classical head wave; the angles of incidence of C_1, C_2, ... have intermediate values. The arrival times of the C_s waves, for small positive values of b and moderate epicentral distances, will differ slightly from that of the classical head wave:

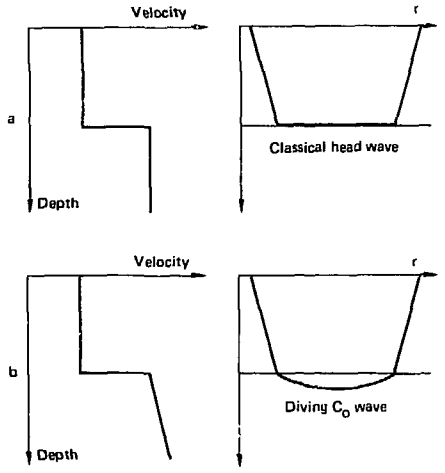

FIG. 3. Two types of velocity distribution below the M discontinuity and the corresponding waves.

$\tau(C_s) < \tau_{131}$ with $\tau(C_s) \to \tau_{131}$ as $s \to \infty$. With increasing epicentral distance, $\tau_{131} - \tau(C_s)$ increases and the individual waves C_0, C_1, C_2, ... will successively separate from the interference wave C+ and exist separately. The C_0 wave will separate first at a distance of [Cerveny and Ravindra, Eq. (6.4)]

$$r_0 = r^*_{131} + (32\alpha_2 \delta t / b^2)^{1/3}. \tag{17}$$

For example, if $\delta t = 0.2$s and $b = 0.002$ km^{-1} and 0.005 km^{-1}, $r_0 = 314$ km and 207 km, respectively.

We now introduce the parameter ζ [Cerveny and Ravindra, Eqs. (6.11, 6.15, 6.16)]:

$$\zeta = (r - r^*_{131}) b^{2/3} (\omega / 2\pi\alpha_2)^{1/3}. \tag{18}$$

Combining Eqs. (17) and (18),

$$\zeta = (32 \delta t \omega / 2\pi)^{1/3}. \tag{19}$$

The quantity $\delta t\omega/2\pi$ is the product of the pulse duration or period and the frequency. If $\delta t\omega/2\pi = 1$, $\zeta_0 = 3.17$.

For $r^*_{131} < r < r_0$, Cerveny and Ravindra [Eqs. (6.24 and 6.25)] give two relations for C+,

$$\bar{W}^{C+} = \bar{W}^{131} Q_2(\zeta) \tag{20}$$

$$\bar{W}^{C+} = \bar{W}^{C} Q_2(\zeta) \tag{21}$$

where Q_2 and $\bar{Q}_2$ are complex functions of ζ. For $\zeta \to 0$ or $r \to r^*_{131}$, $Q_2(\zeta) \simeq 1$ so $\bar{W}^{C+} \to \bar{W}^{131}$. In other words, the properties of the interference head wave C+ are similar to those of the classical head wave in the vicinity of the critical distance r^*_{131}. For $\zeta \to \zeta_0$ such that $r \to r_0$, $Q_2 \to Q_1$, another complex function of ζ. For $\zeta \geq 3$, $|Q_1| \simeq 1$ and $\operatorname{Arg} \bar{Q}_1 \simeq 0$ (Cerveny and Ravindra, Fig. 6.4) so $\bar{W}^{C+} \to \bar{W}^{C}$ as $r \to r_0$. Therefore, the C+ wave is dominated by the C_0 wave at distances approaching those at which C_0 separates from C+. This is because most of the energy of C+ is contributed by C_0. An approximate relation between $\bar{W}^{Cs}$ and $\bar{W}^{131}$ is [Cerveny and Ravindra, Eq. (6.18) for $s = 0$]

$$\bar{W}^{C} = \bar{W}^{131} \pi \zeta^3 \exp\left[\frac{i\pi}{2}\left(1 + \frac{\zeta^3}{6}\right)\right]. \tag{22}$$

From Eqs. (10), (18), and (22),

$$\bar{W}^{C_0} = \frac{\alpha_1 \Gamma_{131} b^2 (r - r^*_{131})^{3/2}}{2i\alpha_2 r^{1/2}}$$

$$\exp\left[\frac{i\omega}{2}\left(1 + \frac{\zeta^3}{6}\right)\right] \exp\left[i\omega(t - \tau_{131})\right] \bar{n}p. \tag{23}$$

The amplitude of the classical head wave [Eq. (10)] is inversely proportional to the frequency ω, but the amplitude of the C_0 wave [Eq. (23)] is independent of frequency. The amplitude of the classical head wave is proportional to $r^{-1/2}(r - r^*_{131})^{-3/2}$ and decreases rapidly with distance. The amplitude of the C_0 wave is proportional to $r^{-1/2}(r - r^*_{131})^{3/2}$ and increases with distance, providing that b is small and r is not too large (obviously, the amplitude of C_0 cannot increase without limit). The C_0 wave will eventually be replaced by the teleseismic P wave as the first arrival.

For our earth model of Fig. 2 (Cerveny and Ravindra, Fig. 6.6), the amplitude of the interference head wave C+ is essentially that of the classical head wave for 80 km $< r <$ 100 km, is a minimum at about $r = 140$ km, and oscillates about that of C_0 for $r >$ 210 km. The C_0 wave emerges from the C+ wave at about $r = 250$ km and is greater in amplitude than the reflected wave $\bar{W}^{11}$ at $r > 260$ km.

From the perspective of regional seismic detection, we may summarize the results of this section, based on the earth model in Fig. 3 as follows and as illustrated in Fig. 4:

- $0 < r < 80$ km. The direct wave is the first arrival which is followed by the reflected wave.
- $r = 80$ km. The head wave exists but is coincident with the reflected wave.
- $105 \text{ km} < r < 130$ km. The head wave emerges in front of the reflected wave but is a secondary arrival relative to the direct wave.
- $r = 140$ km. The interference head wave amplitude is at a minimum; that of the classical head wave continues to decrease with r.
- $r = 180$ km. The head wave (classical or interference) is coincident with the direct wave and emerges as the first arrival at greater r.

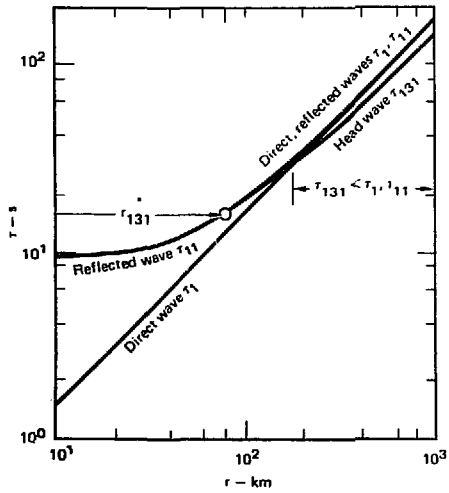

FIG. 4. Travel times for direct, reflected, and head waves for the earth model in Fig. 2.

- $r = 250$ km. The diving wave C_0 separates from the interference head wave.
- $r > 260$ km. The diving wave C_0 is greater in amplitude than the reflected wave.

Let us assume that our model in Fig. 2 is an approximation of reality. We may conclude that if the classical head wave occurs in nature, it will not be of much use for detection purposes because its amplitude is very small compared to those of the direct and reflected waves at distances such that Pn is the first arrival. The formation of the interference head wave is more likely, but it will probably be observed as Pn over a relatively short range of distances (approximately 180 to 250 km in our model of Fig. 2) where it is the first arrival. The diving wave C_0 will probably be observed as Pn at greater distances. This means that most regional signals observed will probably have the source amplitude spectrum $|A(i\omega)|$ and not the head wave spectrum $|A(i\omega)/i\omega|$, neglecting anelastic and other frequency-dependent attenuation.

SEISMIC NOISE SPECTRUM

Seismic noise spectra for frequencies greater than 1 Hz are given by *Brune and Oliver* (1959), *Frantti et al.* (1962), *Frantti* (1963), and *Fix* (1972). Based on these references, we assume the following zero-to-peak seismic noise spectrum for 1 to 20 Hz:

$$|An(2\pi if)| = [2\pi f^{1.5}]^{-1} 10^{-8} \text{ [m/Hz]} . \quad (24)$$

This empirical relation is representative of a quiet, but not the quietest, site. We should note that the exponent for the frequency f varies from approximately −1 for noisy sites to about −2 for very quiet sites.

FREQUENCY FOR MAXIMUM SIGNAL-TO-NOISE RATIO

We assume a seismic source spectrum with a constant-amplitude spectrum $|\hat{A}s(2\pi if)|$ in the frequency band from 1 to 20 Hz. We also assume constant-Q anelastic attenuation. The signal spectra for direct, reflected, and diving waves (Pg, $\bar{P}$, and *certain* Pn waves) are given by the relation

$$\frac{|\hat{A}_s(2\pi if)|}{|\hat{A}_s(f=1)|} = \exp[\pi(1-f)\tau/\bar{Q}_\alpha] , \qquad (25a)$$

where

$|\hat{A}(f=1)|$ = reference signal amplitude at 1 Hz,
f = frequency (Hz),
$\bar{Q}_\alpha$ = mean Q_α for signal path,
τ = signal travel-time.

For the classical and interference head waves (*other* Pn waves), Eq. (25a) must be divided by frequency [see Eq. (10)], so that

$$\frac{|\hat{A}_s(2\pi if)|}{|\hat{A}_s(f=1)|} = (2\pi f)^{-1}\exp[\pi(1-f)\tau/\bar{Q}_\alpha] . \qquad (25b)$$

Similarly, the noise spectrum [Eq. (24)] may be written in the form

$$\frac{|\hat{A}_n(2\pi if)|}{|\hat{A}_n(f=1)|} = f^{-n} \qquad (26)$$

where n, as noted in the preceding section, ranges from 1 to 2 with a preferred value of 1.5.

Then the signal-to-noise ratio, relative to that at a frequency of 1 Hz, is

$$SNR(f) = f^n \exp[\pi(1-f)\tau/\bar{Q}\alpha] \qquad (27a)$$

from Eqs. (25a) and (26), and

$$SNR(f) = (f^{n-1}/2\pi)\exp|\pi(1-f)\tau/\bar{Q}\alpha] \qquad (27b)$$

from Eqs. (25b) and (26). After differentiating Eqs. (27a) and (27b) with respect to f and setting the results equal to zero, we find the following solutions for the frequency corresponding to the maximum signal-to-noise ratio:

$$f(SNR_{max}) = n\bar{Q}\alpha/\pi\tau \qquad (28a)$$

$$f(SNR_{max}) = (n-1)\bar{Q}_\alpha/\pi\tau. \qquad (28b)$$

Therefore, the frequency for SNR_{max} for the classical and interference head waves [Eq. (28b)] is distinctly different from and is less than that for the other regional compressional waves of interest. Solutions for Eqs. (28a) and (28b) are presented in Fig. 5. Note that frequencies up to 20 Hz are optimum for detection of direct, reflected and diving waves under some conditions [Fig. (5a)], but that the optimum frequencies for detection of the classical head wave are less than 10 Hz for the range of conditions considered [Fig. (5b)].

DETECTION OF REGIONAL P WAVES FROM DECOUPLED EXPLOSIONS

As shown previously, the classical and interference head waves (Pn) are not as significant for seismic detection at regional distances as are the direct, reflected, and diving waves — which can be observed as Pg, $\bar{P}$ (for multiple reflections), and Pn, respectively. In the following analysis, we use a source function that is common to the direct, reflected, and diving waves, but we use the propagation function for the direct wave. The results may be realistic, though approximate, for Pg at near-regional distances but are more uncertain for $\bar{P}$ and Pn at regional distances. However, the main purpose of the following analysis is to demonstrate the relative usefulness of different frequencies for seismic detection at regional distances, and not to estimate explosion yields that may be associated with a given signal strength.

We assume that an explosion in a spherical decoupling cavity in an elastic medium may be modeled by a step change in cavity pressure. The

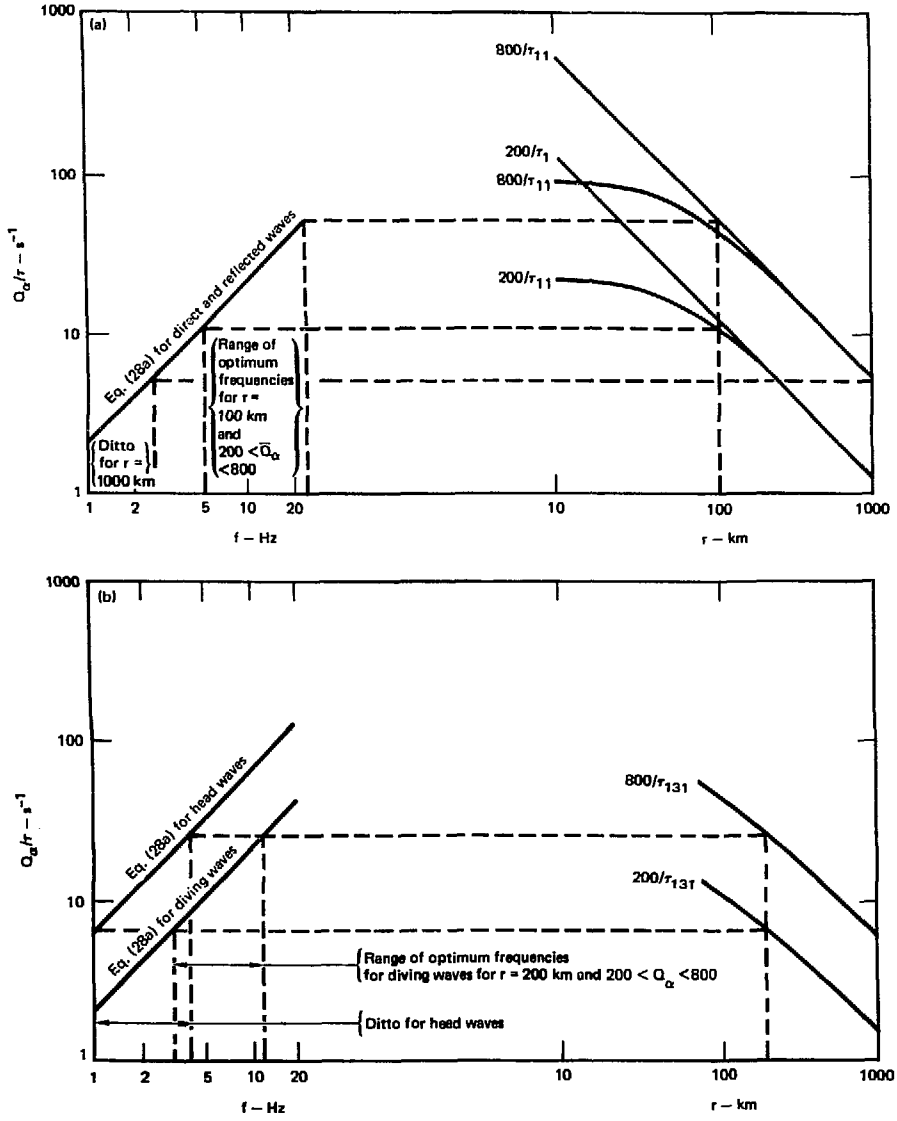

FIG. 5. (a) Optimum frequencies for regional detection of direct and reflected waves; (b) optimum frequencies for regional detection of head and diving waves.

elastic-medium transfer function relating the output $\hat{X}(i\omega)$ to the input $\hat{P}(i\omega)$ is

$$i\omega\hat{X}(i\omega) = \frac{PR^3}{4\mu}\left[1 - \frac{R\omega^2}{4\beta^2} + \frac{iR\omega}{\alpha}\right]^{-1}, \quad (29)$$

where

P = step change in cavity pressure,
R = cavity radius,
$\hat{X}$ = Fourier amplitude of the reduced displacement potential,
α = compressional wave velocity in the elastic medium,
β = shear wave velocity in the elastic medium,
μ = shear modulus of the elastic medium,
ω = angular frequency.

Inspection of the right-hand side of Eq. (5) shows two convenient definitions for a characteristic dimensionless frequency, $R\omega/\alpha$ and $R\omega/2\beta$. The former is used by *Blake* (1952) and *Mueller and Murphy* (1971); the latter by *Gurvich* (1965) and *Rodean* (1971). The two are numerically equal if Poisson's ratio $\nu = 1/3$; they are approximately equal for most solid earth materials. We use

$$\omega_0 = 2\beta/R \quad (30)$$

in our analysis. For frequencies $\omega \leqslant \omega_0$, Eq. (29) may be approximated as

$$i\omega\hat{X}(i\omega) = PR^3/4\mu. \quad (31)$$

The displacement amplitude spectrum for spherical compressional waves in an extended, homogeneous, isotropic elastic medium is related to the spectrum of the reduced displacement potential as

$$\hat{A}p(r,i\omega) = -\left(\frac{i\omega}{\alpha r} + \frac{1}{r^2}\right)\hat{X}(i\omega), \quad (32)$$

where

$\hat{A}p$ = Fourier amplitude of the displacement,
r = radial or epicentral distance from the center of the source.

We assume the far-field term in Eq. (32) is appropriate for the direct P wave. The displacement spectrum for $\omega \leqslant \omega_0$ is, then, from Eqs. (31) and (32),

$$|\hat{A}p(r,i\omega)| = PR^3/4\mu\alpha r. \quad (33)$$

This relation is equivalent to Eq. (5) for Pg and is approximately equivalent to Eq. (7) for $\bar{P}$.

Our assumed decoupling cavity is in salt, and our assumed propagation path is in granite. If we assume normal incidence of the seismic waves upon the salt-granite interface, the ratio of the displacement amplitudes of the incident and the transmitted P waves is *(Kolsky*, 1963)

$$\frac{Ap_2}{Ap_1} = 2\left(1 + \frac{\rho_2\alpha_2}{\rho_1\alpha_1}\right)^{-1}, \quad (34)$$

where

ρ medium density,
1 first medium (salt),
2 second medium (granite).

If we also assume constant-Q anelastic attenuation, the observed P-wave amplitude spectral density for $\omega \leqslant \omega_0$ is, from Eqs. (33) and (34),

$$|\hat{A}p(r,2\pi if)| = \frac{PR^3}{4\pi\mu\alpha_2 r}\left(1 + \frac{\rho_2\alpha_2}{\rho_1\alpha_1}\right)^{-1} \times \exp - \frac{\Delta\pi f}{\alpha_2 Q_\alpha}. \quad (35)$$

For an assumed signal-to-noise ratio of 1.5 for signal detection, Eqs. (24) and (35) may be combined to give

$$\frac{P}{\mu} = \frac{3\alpha_2 r}{10^8 f^{1.5} R^3}\left(1 + \frac{\rho_2\alpha_2}{\rho_1\alpha_1}\right)\exp\frac{\Delta\pi f}{\alpha_2 Q_\alpha}. \quad (36)$$

where P/μ is a convenient, dimensionless, decoupling-cavity operating parameter. Solutions of Eq. (36) are presented in Fig. 6. It is shown that the higher frequencies (10 to 20 Hz) are more useful for detection at near-regional distances out to a few hundred kilometers, and that frequencies of 5 to 10 Hz are more useful at regional distances approaching 1,000 km. The scale on the right-hand side of Fig. 6 indicates the values of explosion yield E corresponding to the indicated values of P/μ according to the relation

$$PV = (\gamma - 1)E, \quad (37)$$

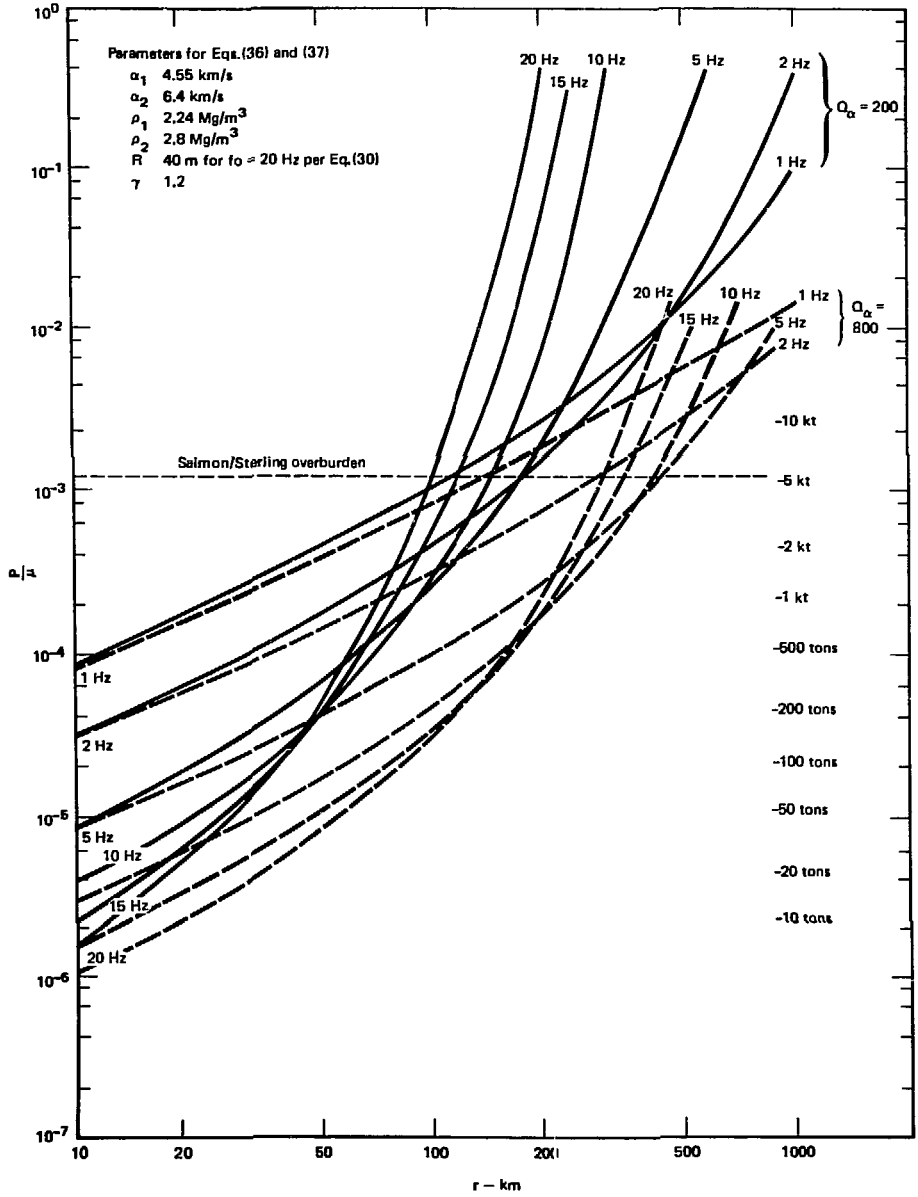

FIG. 6. Decoupling cavity conditions for Pg detection vs epicentral distance with frequency Q as parameters.

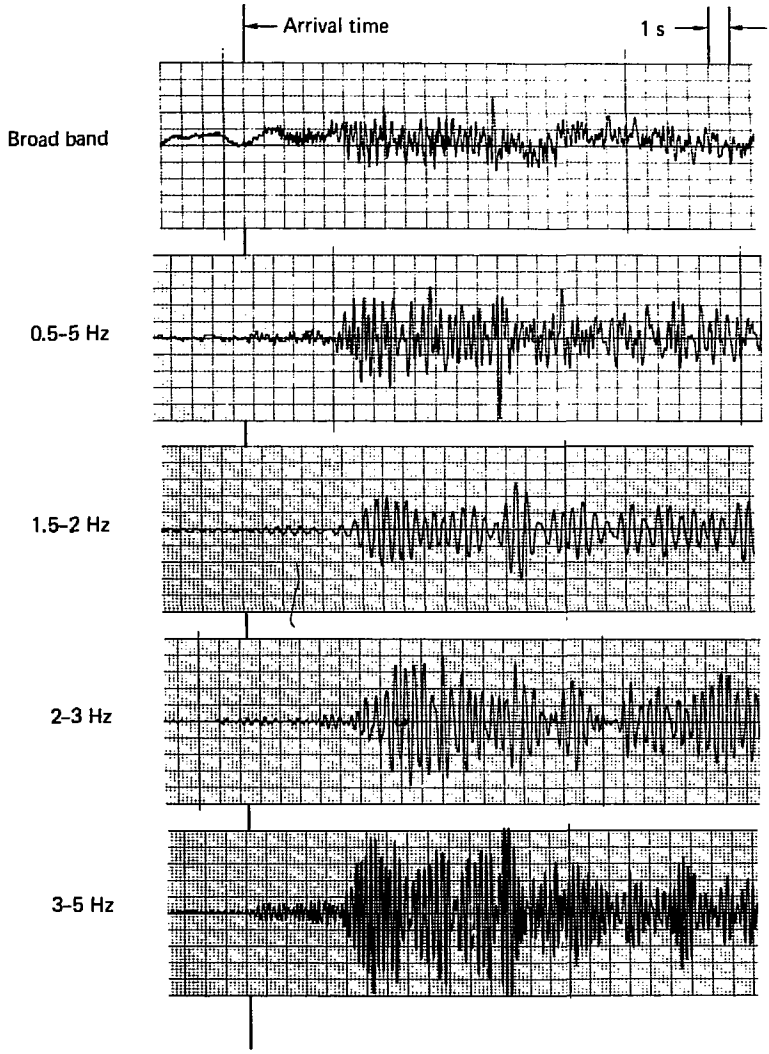

FIG. 7. Recording at Kanab, Utah, of a 0.5-kt test in Yucca Flat above the water table.

where

V = cavity volume,

γ = ratio of enthalpy to internal energy for the explosion gases.

In closing, we consider one regional seismogram presented in Fig. 7 (*D. L. Springer*, 1977). The event was a 0.5 kt nuclear explosion in dry alluvium above the water table in Yucca Flat at the Nevada Test Site. The recording was made at an epicentral distance of approximately 300 km at the LLL seismic station near Kanab, Utah. The top section of Fig. 7 shows the original broadband recording (flat in velocity response from 0.05 to 20 Hz). The remainder of the figure shows the results of bandpass filtering of the original broadband recording. The second arrival, Pg($\bar{P}$), which appears about 5 s after the indicated signal arrival time, is fairly noticeable on all sections of Fig. 7. However, the first arrival, Pn, is distinct in only the highest frequency band shown (3 to 5 Hz). Pg($\bar{P}$) is also more distinct in this frequency band. We may conclude that the data in Fig. 7 are consistent with the theoretical results shown in Figs. 5 and 6.

CONCLUSIONS

The classical and interference head waves are probably observed as Pn over a relatively restricted epicentral range and at less-favorable signal-to-noise ratios than the other regional P waves. The most useful crustal P waves for regional seismic detection are the direct (observed as Pg), reflected (multiply reflected in the case of the observed $\bar{P}$), and diving (also observed as Pn) waves. The theoretical amplitudes of the classical and interference head waves are generally significantly smaller than those of direct, reflected, and diving waves.

The source spectra of the classical and interference head waves are proportional to those of the direct, reflected, and diving waves divided by the frequency. Therefore the signal-to-noise ratios for the classical and interference head waves are less favorable than those for the other regional P waves if the seismic noise spectrum varies inversely as a power greater than unity of the frequency.

Frequencies of 10 to 20 Hz are more useful for seismic detection at near-regional distances of a few hundred km; frequencies of 5 to 10 Hz are more useful at regional distances up to 1,000 km.

APPENDIX: CAVITIES IN SALT

Salt deposits, especially salt domes, are a favored location for decoupling cavities because salt deposits are relatively free of strength-limiting joints and faults that adversely affect cavity stability. This salt deposit property is demonstrated by the fact that, of the several hundred underground nuclear explosions detonated by the United States, only the 3-kt Gnome and the 5.3-kt Salmon events in salt are known to have produced standing cavities. Two nuclear explosions detonated by the USSR in salt with yields of 1.1 and 25 kt also produced stable cavities. The Cowboy decoupling experiments with high explosives were conducted in a salt mine. The Sterling nuclear decoupling experiment was conducted in the cavity formed by the Salmon event.

Some data pertinent to our study of decoupling cavities are presented in Table A-1. Note that only preshot physical properties of the Salmon salt are presented. Considerable uncertainty remains concerning the characteristics of the post-Salmon salt properties that formed the Sterling environment (*Sisemore et al.* 1966). Therefore, in this study we assumed mined decoupling cavities, not shot-formed cavities.

TABLE A-1. Properties and conditions of preshot Salmon cavities in salt.[a]

Parameter	Value	How obtained
Bulk density[b] (ρ), kg/m^3	2.24×10^3	Measured
Bulk modulus (k), N/m^2	2.74×10^{10}	Calculated
Shear modulus (μ), N/m^2	1.42×10^{10}	Calculated
Compressional wave velocity[b] (α), m/s	4,550	Measured
Shear wave velocity[b] (β), m/s	2,520	Measured
Poisson's ratio (ν)	0.28	Calculated
Salmon overburden pressure[c], N/m^2	1.81×10^7	Calculated

[a]The cavity radii were as follows: 5.3-kt Salmon – 17.4m (*Rawson et al.*, 1966); 25-kt Soviet PNE – 33m (*Kedrovskiy*, 1970); for f_0 = 20 Hz [from Eq. (30)] – 40 m.

[b]*Rawson et al.* (1966).

[c]*Rogers* (1966); calculated for the shot point depth of 827.8 m.

REFERENCES

1. M. Bäth, *Introduction to Seismology,* (Birkhauser Verlag, Basle, 1973).
2. M. J. Berry and G. F. West, "Reflected and Head Wave Amplitudes in a Medium of Several Layers," *The Earth Beneath the Continents,* eds. J.S. Steinhart and T. J. Smith (American Geophysical Monograph 10, Washington, D. C., 1966), pp. 464-481.
3. F. G Blake, Jr., "Spherical Wave Propagation in Solid Media," *J. Acoust. Soc. Am.* **24**, 211-215 (1952).
4. J. N. Brune and J. Oliver, "The Seismic Noise of the Earth's Surface," *Bull. Seismol. Soc. Am.* **49**, 349-353 (1959).
5. V. Cerveny, "On Dynamic Properties of Reflected and Head Waves in the N-Layered Earth's Crust," *Geophys. J. R. Astr. Soc.* **11**, 139-147 (1966).
6. V. Cerveny and R. Ravindra, *Theory of Seismic Head Waves* (University of Toronto Press, Toronto, 1971).
7. Z. A. Der and T. W. McElfresh, "The Relationship Between Anelastic Attenuation and Regional Amplitude Anomalies of Short-Period P Waves in North America, *Bull. Seismol. Soc. Am.* **67**, 1303-1317 (1977).
8. J. F. Evernden, "Magnitude Determination at Regional and Near-Regional Distances in the United States," *Bull. Seismol. Soc. Am.* **57**, 591-639 (1967).
9. W. M. Ewing, W. S. Jardetzky, and F. Press, *Elastic Waves in Layered Media* (McGraw-Hill, New York, 1957).
10. J. Fix, "Ambient Earth Motion in the Period Range from 0.01-2560s," *Bull. Seismol. Soc. Am.* **62**, 1753-1760 (1972).
11. G. E. Frantti, "The Nature of High-Frequency Earth Noise Spectra," *Geophysics* **28**, 547-562 (1963).
12. G. E. Frantti, D. E. Willis, and J. T. Wilson, "The Spectrum of Seismic Noise," *Bull. Seismol. Soc. Am.* **52**, 113-121 (1962).
13. I. I. Gurvich, *"The Theory of Spherical Radiation of Seismic Waves," Izv. Akad. Nauk SSSR, Ser. Fiz. Zemli,* No. 10, 45-56 (1965) (Bull. Acad. Sci. USSR, Earth Physics, No. 10, 684-689).
14. N. A. Haskell, "The Leakage Attenuation of Continental Crustal P Waves," *J. Geophys. Res.* **71**, 3955-3967 (1966).
15. R. B. Herrmann and B. J. Mitchell, "Statistical Analysis and Interpretation of Surface-Wave Anelastic Attenuation Data for the Stable Interior of North America," *Bull. Seismol. Soc. Am.* **65**, 1115-1128 (1975).
16. D. P. Hill, "Velocity Gradients and Anelasticity from Crustal Body Wave Amplitudes," *J. Geophys. Res.* **76**, 3309-3325 (1971).
17. D. P. Hill, "Critically Refracted Waves in a Spherically Symmetric Radially Heterogeneous Earth Model," *Geophys. J. R. Astr. Soc.* **34**, 149-177 (1973).
18. O. L. Kedrovskiy, *Prospective Applications of Underground Nuclear Explosions in the National Economy of the USSR,* Lawrence Livermore Laboratory Rept. UCRL-Trans-10477 (1970). Translation from the Russian of three papers (IAEA-PL-388/19, 20, 21) published in *Peaceful Nuclear Explosions, Phenomenology and Status Report, 1970* by the International Atomic Energy Agency, Vienna (1970).
19. H. Kolsky, *Stress Waves in Solids* (Dover Publications, Inc., New York, 1963).
20. R. A. Mueller and J. R. Murphy, "Seismic Characteristics of Underground Nuclear Detonations. Part I. Seismic Spectrum Scaling," *Bull. Seismol. Soc. Am.* **61**, 1675-1692 (1971).
21. I. L. Nersesov and T. G. Rautian, Kinematics and Dynamics of Seismic Waves at Distances up to 3500 km from Epicenter," Akad. Nauk SSSR, *Trudy Inst. Fiziki Zemli* **32**(199), 63-87 (1964).
22. O. W. Nuttli, "A Time-Domain Study of the Attenuation of 10-Hz Waves in the New Madrid Seismic Zone," *Bull. Seismol. Soc. Am.* **68**, 343-355 (1978).
23. F. Press, "Seismic Attenuation in the Crust," *J. Geophys. Res.* **69**, 4417-4418 (1964).
24. D. Rawson, P. Randolph, C. Boardman, and V. Wheeler, "Post-Shot Environment Resulting from the Salmon Event," *J. Geophys. Res.* **71**, 3507-3521 (1966).

25. H. C. Rodean, *Nuclear-Explosion Seismology* (U.S. Atomic Energy Commission, Oak Ridge, Tenn., 1971).
26. L. A. Rogers, "Free-Field Motion Near a Nuclear Explosion in Salt: Project Salmon," *J. Geophys. Res.* **71**, 3415-3467 (1966).
27. C. J. Sisemore, L. A. Rogers, and W. R. Perret, Project Sterling: "Subsurface Phenomenology Measurements Near A Decoupled Nuclear Event," *J. Geophys. Res.* **74**, 6623-6637 (1969).
28. D. Springer, Lawrence Livermore Laboratory, private communication (1977).
29. D. Springer, M. Denny, J. Healy, and W. Mickey, "The Sterling Experiment: Decoupling of Seismic Waves by a Shot-Generated Cavity," *J. Geophys. Res.* **73**, 5995-6011 (1968).
30. G. C. Werth, R. F. Herbst, and D. L. Springer, "Amplitudes of Seismic Arrivals from the M Discontinuity," *J. Geophys. Res.* **67**, 1587-1610 (1962).